Coupled states of cold ^{174}Yb atoms in a high-finesse cavity

Saran Shaju,[1] Dmitriy Sholokhov,[1] Simon B. Jäger,[2] and Jürgen Eschner[1,*]
[1]*Experimentalphysik, Universität des Saarlandes, 66123 Saarbrücken, Germany*
[2]*Physics Department and Research Center OPTIMAS, University of Kaiserslautern-Landau, 67663 Kaiserslautern, Germany*

(Received 9 August 2024; revised 3 December 2024; accepted 2 June 2025; published 7 July 2025)

We experimentally and theoretically study the formation of dressed states emerging from strong collective coupling of the narrow intercombination line of Yb atoms to a single mode of a high-finesse optical cavity. By permanently trapping and cooling the Yb atoms during their interaction with the cavity, we gain continuous experimental access to the dressed states. This allows us to detect both their field and their atomic properties, by simultaneously measuring the steady-state cavity transmission and free-space fluorescence. By varying the cavity and probe frequencies, we observe coupled atom-cavity states with atom-number-dependent splitting, the hallmark of collective strong coupling of the atoms with the single cavity mode. We find additional fluorescence output at atomic resonance, which we explain by the effects of dephasing and inhomogeneous broadening. We compare our experimental results with a theoretical model and find good qualitative agreement.

DOI: 10.1103/8k18-9mvn

I. INTRODUCTION

Cold atomic ensembles in optical cavities are a versatile platform to study collective effects such as self-organization [1–6], super- and subradiance [7–15], and in general long-range or even arbitrary cavity-mediated interactions [16–20]. Based on these effects, various applications have been proposed, ranging from quantum simulators and computers [21–23] to ultraprecise lasers and active optical clocks [24–28]. Trapping light in the confined geometry of an optical cavity massively enhances the interaction between a photon and a single atom. In the presence of many atoms, this interaction is in addition collectively enhanced, which allows for very strong light-matter interactions and the achievement of very large collective linewidths even when working with atoms that possess very narrow natural linewidths due to the constructive interference of their emission amplitudes. With this, one can work in a regime where very strong nonlinearities can be generated while unwanted decoherence channels such as spontaneous emission are weak, which is an ideal ground for future quantum technologies.

However, this field faces a major challenge which arises from atomic motion inducing line broadening and also eventually the loss of atoms. Cooling and trapping [29] of the atoms in a regime where the total broadening is smaller than the collectively enhanced coupling strength is a minimum requirement. In several experiments this is achieved in a sequential way where first the gas is cooled and prepared in a trap and then one investigates collective effects emerging from the atom-cavity coupling in a second step. In this second step the atoms will heat, which leads to the loss of atoms and sets the time limit on which operations can be performed. This is a major limitation and only recently several groups investigating light-matter interaction with narrow linewidth atoms have proposed [26,30–35] and realized [36,37] the operations of such devices in a continuous regime where atoms are constantly refilled. An alternative to such atomic beam configurations is to achieve continuous operation due to simultaneous trapping and cooling that counteract adverse heating effects. The possibility to achieve with this continuous lasing on a narrow line has been proposed by several theoretical groups [38–42] and partially realized in experiment [43,44]. An open question here is to understand the formation of dressed states between the narrow-line atomic transition and the optical cavity mode. In particular, it has not been explored experimentally how broadening due to motion and incoherent light scattering affects the spectral features of the emerging dressed states.

In this paper we address this question by experimentally and theoretically investigating the dressed states formed by strong collective coupling between the $^1S_0 \leftrightarrow {}^3P_1$ intercombination line of ^{174}Yb atoms and a resonant optical cavity. The formation of dressed states has been studied in several works ranging from single-atom experiments [45–52] to atomic ensembles [50,53–56]. More recently, these studies have also been extended to narrow intercombination lines [33,57,58]. In contrast to these studies, we observe the dressed states in a fully continuous fashion which is facilitated by simultaneous cooling and trapping with a magneto-optical trap on the $^1S_0 \leftrightarrow {}^1P_1$ transition. Besides the fundamental interest in such continuous collective coupling regimes, it also allows us to efficiently collect and analyze free-space fluorescence from the narrow transition over several seconds.

Over such long timescales, we detect the photonic and the atomic character of the dressed states by measuring the cavity transmission and by detecting the fluorescence from the narrow intercombination line, respectively. We compare

*Contact author: juergen.eschner@physik.uni-saarland.de

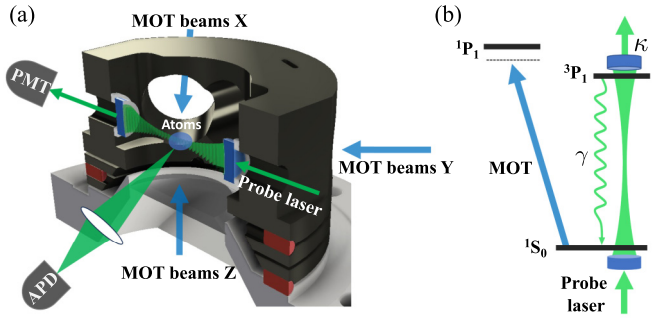

FIG. 1. (a) Schematic of the experimental setup for probing the atom-cavity coupled states. Atoms are held by a conventional three-dimensional MOT on the $^1S_0 \leftrightarrow {}^1P_1$ blue line and a laser drive is provided along the cavity axis. The cavity transmission is detected using a photomultiplier tube (PMT) and an avalanche photodetector (APD) is used for counting the fluorescence photons emitted by the atoms into free space. (b) The atomic level scheme shows the relevant transitions for the experiment, where the atoms are held using the broad blue transition and the atom-cavity interaction is on the narrow $^1S_0 \leftrightarrow {}^3P_1$ intercombination line.

these measurements to theoretical predictions that include inhomogeneous broadening of the narrow atomic line. We find qualitative good agreement for realistic atom numbers and broadening. Our work is a step towards exploring the behavior of narrow-linewidth atoms strongly coupled to optical cavities while they are continuously trapped on a broader line, which is a possible scenario for their use in quantum technologies.

This paper is structured as follows. In Sec. II we describe the experimental setup, while Sec. III introduces our theoretical tools. In Sec. IV we report the measurements of the cavity-field transmission and the free-space fluorescence and compare them to theory. In Sec. V we summarize our results and discuss our conclusions.

II. EXPERIMENTAL SETUP AND MEASUREMENT PROTOCOL

A. Lasers

Two lasers are employed. One is used for cooling and trapping the Yb atoms in a conventional six-beam magneto-optical trap (MOT) on the $^1S_0 \leftrightarrow {}^1P_1$ dipole-allowed transition at $\lambda_{\mathrm{MOT}} = 399$ nm (so-called blue transition, linewidth $\gamma_{\mathrm{MOT}} = 2\pi \times 29.1$ MHz). The other laser is nearly resonant with the $^1S_0 \leftrightarrow {}^3P_1$ intercombination line at $\lambda = 556$ nm (so-called green transition, linewidth $\gamma = 2\pi \times 182.4$ kHz); it is used as a probe to drive the atom-cavity system through a cavity mirror. The blue laser is frequency stabilized via a transfer locking scheme [59] and the green laser is stabilized to the green transition by atomic-beam spectroscopy. Both lasers are tuned with acousto-optical modulators (AOMs). The relevant transitions are displayed in Fig. 1(b).

B. Atoms

In the experiment we work with ^{174}Yb atoms that are evaporated from an oven operating at 500 °C. The collimated atoms are guided to a MOT and slowed down by a Zeeman slower operating on the $^1S_0 \leftrightarrow {}^1P_1$ transition. The MOT, typically operating at $\Delta_{\mathrm{MOT}} = -2\pi \times 30$ MHz with a total optical power of 6.5 mW, traps and cools the atoms in a spatial region approximately 1 mm in size around the center of our optical cavity [see Fig. 1(a)]. In the overlap region between the MOT and cavity mode, about 10^4–10^5 atoms are held at a temperature of 5–10 mK.

C. Cavity

The high-finesse optical cavity has a length of $L = 4.78$ cm in the Fabry-Pérot configuration and waist radius of 87 μm in the TEM_{00} mode. It couples to the $^1S_0 \leftrightarrow {}^3P_1$ atomic transition at $\lambda = 556$ nm, where it has a loss rate of $\kappa = 2\pi \times 70$ kHz (finesse $\mathcal{F} = 45\,000$). A single atom in this setup couples to the cavity with a vacuum Rabi frequency $g_0 = 2\pi \times 66$ kHz, corresponding to a single-atom cooperativity $C_1 = g_0^2/\kappa\gamma = 0.34$ [60]. By trapping a large number N of atoms in the cavity mode, collective strong coupling $C = NC_1 \gg 1$ is achieved, which leads to the formation of atom-cavity coupled states in the system that we investigate. Nevertheless, since the beam waist of the cavity is small compared to the size of the cloud itself, only a small percentage of the total number of atoms interact with the cavity.

The cavity length is stabilized by locking it to a reference derived from the green laser. In our setup, we use a reference beam which is 0.4 GHz shifted from the green transition frequency and resonant to the 15th transverse mode of the cavity. Feedback is applied to piezoelectric actuators attached to the cavity mirrors. The uncertainty of the cavity frequency is on the order of the cavity linewidth. The cavity frequency is then controlled by shifting the frequency of the reference beam with an AOM.

D. Detection

Detection in our setup happens in two channels: first, detection of the cavity transmission, and second, detection of the atomic fluorescence emitted into free space. The transmitted light from the cavity is collected to a single-mode fiber and detected with a photomultiplier tube (PMT). In the figures shown below, 1 mV of the PMT signal translates to about 70 pW of cavity output, or approximately 4×10^4 photons inside the cavity. Fluorescence is recorded using a telescope imaging scheme with a pair of 1-in. lenses to collect and collimate the photons, which are then fiber coupled to an avalanche photodetector (APD) in counting mode. A color filter rejects the blue MOT fluorescence.

E. Measurement protocol

The measurement begins with loading the atoms into the MOT, tracking the fluorescence at 399 nm as a measure of number of atoms trapped. The atomic flux to the MOT is regulated using a motorized mechanical shutter. Using this, we control the number of atoms that interact with the cavity. The cloud position is adjusted by the MOT beam directions and powers and monitored with CCD cameras to ensure the geometrical overlap with the cavity mode. Once good overlap is attained that supports the formation of the atom-cavity states, the cavity is driven with the probe laser. The intensity

of the probe is chosen such that it leads to an intracavity power of 100 μW.

With the atoms inside the cavity, we set the detuning of the cavity to a fixed value Δ_c and scan the frequency of the probe laser Δ_p. For each parameter set (Δ_c, Δ_p) we measure the cavity transmission and free-space fluorescence using the PMT and APD, respectively, for 5–10 s to obtain a good signal-to-noise ratio.

We emphasize some aspects in which our experimental situation is peculiar and regarding which our results are novel. First, the atom-cavity states are subject to dephasing induced by (i) the MOT beams and (ii) the strong saturation of the green transition inside the cavity. Second, on the scale of the cavity and atomic linewidth, there is significant inhomogeneous (Doppler) broadening due to the MOT temperature. To overcome these effects, we trap a large number of atoms and produce a Rabi splitting nearly two orders of magnitude larger than the linewidth. Finally, by measuring the fluorescence when the strong probe is inside the cavity, we not only observe the cavity transmission but also have simultaneous access to the atomic response of the coupled system.

III. THEORETICAL DESCRIPTION

A. Mean-field description

We use a mean-field description for the dynamics of N two-level atoms with the internal ground (excited) state $|g\rangle$ ($|e\rangle$) interacting with the driven cavity mode. This model is a generalization of disordered spin systems which have been connected to the formation of dark states in cavities [61–65]. In our approach we replace all quantum operators by their expectation values. The equations of motion describing the coupled driven-dissipative atom-cavity dynamics are given by

$$\frac{d\alpha}{dt} = \left(i(\Delta_p - \Delta_c) - \frac{\kappa}{2}\right)\alpha - i\frac{\eta}{2} - i\frac{g_0}{2}\sum_j s_j, \tag{1}$$

$$\frac{ds_j}{dt} = \left(i(\Delta_p - \omega_j) - \frac{\gamma + \gamma_d}{2}\right)s_j + i\frac{g_0}{2}\alpha z_j, \tag{2}$$

$$\frac{dz_j}{dt} = -\gamma(1 + z_j) + ig_0(\alpha^* s_j - s_j^*\alpha), \tag{3}$$

where $\alpha = \langle\hat{a}\rangle$, $s_j = \langle\hat{\sigma}_j^-\rangle$, and $z_j = \langle\hat{\sigma}_j^z\rangle$ are the mean values of the cavity-field annihilation operator $\hat{a}$, the lowering operator $\hat{\sigma}_j^- = |g\rangle_j\,{}_j\langle e|$, and the inversion operator $\hat{\sigma}_j^z = |e\rangle_j\,{}_j\langle e| - |g\rangle_j\,{}_j\langle g|$, respectively. This description is derived in a frame rotating with the laser frequency ω_L, and we have introduced the respective detunings between cavity and atom $\Delta_c = \omega_c - \omega_a$ and between laser and atom $\Delta_p = \omega_p - \omega_a$. In Eq. (1) we have introduced the cavity linewidth κ, the cavity-field driving amplitude η, and the vacuum Rabi frequency g_0. The frequencies governing the dynamics of the atomic degrees of freedom [Eqs. (2) and (3)] are the natural atomic linewidth γ, homogeneous dephasing γ_d, and an atom-dependent frequency ω_j which is drawn from a distribution function

$$f(\omega) = \frac{1}{\sqrt{2\pi\,\Delta\omega^2}}e^{-\omega^2/(2\Delta\omega^2)}. \tag{4}$$

Inhomogeneous broadening described by $\Delta\omega$ and homogeneous dephasing described by γ_d is introduced to model several effects in our experiment including Doppler broadening, magnetic shifts, and random motion introduced by the MOT.

Equations (1)–(3) are the basis of our theoretical analysis, and in the following we will derive the stationary state which is used for comparison to the experimental results.

B. Stationary state

We will now derive the stationary state of Eqs. (1)–(3). We are interested in both the cavity field and the excited-state population, which are accessed in the experiment by measuring the cavity transmission and the atomic fluorescence, respectively.

We find the stationary solution of Eq. (2), which reads

$$s_j = \frac{-\frac{g_0}{2}z_j}{(\Delta_p - \omega_j) + i\frac{\gamma+\gamma_d}{2}}\alpha. \tag{5}$$

Using this result in Eq. (3) and imposing $dz_j/dt = 0$, we obtain the steady-state expression for z_j, which takes the form

$$z_j = -\frac{1}{1 + \frac{\frac{g_0^2|\alpha|^2(\gamma+\gamma_d)}{2\gamma}}{(\Delta_p-\omega_j)^2 + \left(\frac{\gamma+\gamma_d}{2}\right)^2}}. \tag{6}$$

With this solution we find s_j [Eq. (5)], which is then used to solve $d\alpha/dt = 0$ in Eq. (1) such that

$$\alpha = \frac{\frac{\eta}{2}}{(\Delta_p - \Delta_c) + i\frac{\kappa}{2} + i\frac{\Gamma}{2}}. \tag{7}$$

Here we introduced

$$\begin{aligned}\Gamma &= i\sum_j \frac{\frac{\frac{g_0^2}{2}}{(\Delta_p-\omega_j)+i\frac{\gamma+\gamma_d}{2}}}{1 + \frac{\frac{g_0^2|\alpha|^2(\gamma+\gamma_d)}{2\gamma}}{(\Delta_p-\omega_j)^2+\left(\frac{\gamma+\gamma_d}{2}\right)^2}} \\ &= i\int_{-\infty}^{\infty} d\omega\,\tilde{f}(\omega)\frac{\frac{\frac{g_0^2}{2}}{(\Delta_p-\omega)+i\frac{\gamma+\gamma_d}{2}}}{1 + \frac{\frac{g_0^2|\alpha|^2(\gamma+\gamma_d)}{2\gamma}}{(\Delta_p-\omega)^2+\left(\frac{\gamma+\gamma_d}{2}\right)^2}}\end{aligned} \tag{8}$$

using the function

$$\tilde{f}(\omega) = \sum_j \delta(\omega - \omega_j). \tag{9}$$

For very large atom numbers N, this function approaches $\tilde{f}(\omega) \to Nf(\omega)$ with the distribution function introduced in Eq. (4). We get then

$$\Gamma = i\int_{-\infty}^{\infty} d\omega\, f(\omega)\frac{\frac{\frac{Ng_0^2}{2}}{(\Delta_p-\omega)+i\frac{\gamma+\gamma_d}{2}}}{1 + \frac{\frac{g_0^2|\alpha|^2(\gamma+\gamma_d)}{2\gamma}}{(\Delta_p-\omega)^2+\left(\frac{\gamma+\gamma_d}{2}\right)^2}}. \tag{10}$$

Note that Γ depends on α, which requires that one has to solve Eq. (7) self-consistently with Eq. (10). For $\Delta_p = 0 = \Delta\omega$ and zero dephasing $\gamma_d = 0$ we have $\Gamma = NC\kappa$, with the cooperativity $C = g_0^2/(\kappa\gamma)$. More generally, Γ represents the line broadening and dispersive shift of the cavity due the presence of the atoms. The result for the cavity field [Eq. (7)] when

using Eq. (10) is equivalent to the result found in Ref. [58] in the limit $\Delta\omega = 0 = \gamma_d$. Finally, we calculate the average photon number leaving the cavity per unit time

$$T = \kappa|\alpha|^2 = \frac{\frac{\eta^2}{4}}{\left|\Delta_p - \Delta_c + i\frac{\kappa}{2} + i\frac{\Gamma}{2}\right|^2} \tag{11}$$

and fluorescent photon number per unit time

$$F = \gamma \sum_j \frac{1+z_j}{2} = \int_{-\infty}^{\infty} d\omega N f(\omega) \frac{\frac{\frac{g_0^2|\alpha|^2(\gamma+\gamma_d)}{4}}{(\Delta_p-\omega)^2+\left(\frac{\gamma+\gamma_d}{2}\right)^2}}{1+\frac{\frac{g_0^2|\alpha|^2(\gamma+\gamma_d)}{2\gamma}}{(\Delta_p-\omega)^2+\left(\frac{\gamma+\gamma_d}{2}\right)^2}}. \tag{12}$$

We solve self-consistently Eqs. (10) and (11) for $|\alpha|^2$, which is then used to calculate the expressions T and F. In the figures shown later we normalize the quantities T and F by the empty cavity transmission $T_0 = \eta^2/\kappa$ and the collective spontaneous decay rate $N\gamma$.

In the next section we use the results of this model and compare them to our experimental data.

IV. COLLECTIVE LIGHT-MATTER STATES

In this section we present the main results, which include the measured cavity transmission and fluorescence and their comparison to the theory described in the preceding section.

A. Measured cavity transmission and fluorescence

In Fig. 2 we show the measured cavity transmission in units of the voltage detected by the PMT [Fig. 2(a)] and the measured fluorescence in units of photon counts measured by the APD [Fig. 2(b)], as functions of the cavity-atom detuning Δ_c and probe-atom detuning Δ_p. Both detunings are varied in a range $2\pi \times (-15, \ldots, 15$ MHz). In the cavity signal shown in Fig. 2(a), we observe transmission for large detunings $|\Delta_c|, |\Delta_p| \geqslant 2\pi \times 10$ MHz and when $\Delta_c \approx \Delta_p$. Closer to atomic resonance, the transmission peaks show an avoided crossing and their magnitude tends to zero. The fluorescence signal, displayed in Fig. 2(b), shows behavior similar to the transmission, but additionally it exhibits a bright central feature close to resonance $\Delta_c \approx 0$ across nearly the whole range of Δ_p. This feature does not appear in the cavity transmission. To understand this behavior better, we apply our theoretical model and show the corresponding numerical results in Figs. 2(c) and 2(d). The cavity transmission displayed in Fig. 2(c) is in good agreement with the experimental data in Fig. 2(a). The physical origin of the avoided crossing is the formation of coupled eigenstates between the atoms and the cavity. The coupled-state resonances are approximately described by

$$\Delta'_{c\pm} = \frac{\Delta_c}{2} \pm \frac{1}{2}\sqrt{\Delta_c^2 + N g_0^2}. \tag{13}$$

We show the result of this formula as a guide to the eye in Figs. 2(a)–2(d) for $N = 25\,000$, which is thereby used to estimate the effective number of atoms participating in the atom-cavity interaction.

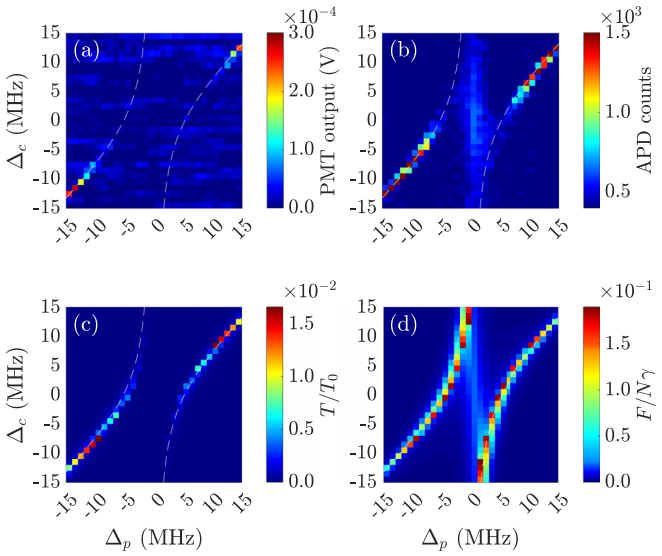

FIG. 2. Atom-cavity coupled states. (a) and (b) Measurement and (c) and (d) theory for (a) and (c) cavity transmission and (b) and (d) fluorescence. (a) Cavity transmission detected with a PMT when an effective atom number of 25 000 is present in the cavity mode. The white dashed line marks the resonance position according to the simple dressed-state formula (13). A background originating mainly from detector noise has been subtracted. (b) Simultaneously measured atomic fluorescence photon counts in 10 s. Atom-cavity coupled states are observed as in the case of cavity transmission. The peculiar feature which appears to be an additional broad resonance is visible around $\Delta_p \approx 0$. Also shown are the calculated normalized (c) cavity transmission T/T_0 [Eq. (11)] and (d) fluorescence $F/(N\gamma)$ [Eq. (12)], when the cavity is driven with $\eta = 2\pi \times 87$ MHz and an inhomogeneous broadening of $\Delta\omega = 2\pi \times 0.9$ MHz and dephasing of $\gamma_d = 2\pi \times 1$ kHz are used.

The coupled states are also visible in the fluorescence [Figs. 2(b) and 2(d)] as their atomic contribution undergoes spontaneous decay into free space. Importantly, in the theory prediction in Fig. 2(d), we also find the central feature close to atom-probe resonance $\Delta_p \approx 0$, which is not part of the formation of atom-cavity coupled states. It will be investigated in more detail in Sec. IV C.

B. Atom-number dependence

Controlling the atomic flux into the trapping volume allows us to extend our experiments and include variation of the atom number. We focus here on showing the fluorescence excited via the probe, measured as in the preceding section but for different numbers of atoms in the cavity mode. Figure 3 shows the results when Δ_c and Δ_p are varied in the same range as in Fig. 2. As we go from Fig. 3(a) to Fig. 3(d), the atom number is increased and correspondingly more splitting is visible. In Fig. 3(a), corresponding to the lowest number of atoms, the fluorescence appears very close to the diagonal, $\Delta_c = \Delta_p$; for the next higher atom number one can observe the beginning of splitting close to the atomic resonance. As we continue to increase the atom number, in Fig. 3(c) a clear splitting is observed, which becomes noticeably wider as we go to Fig. 3(d). In the latter two maps, the splitting is accompanied

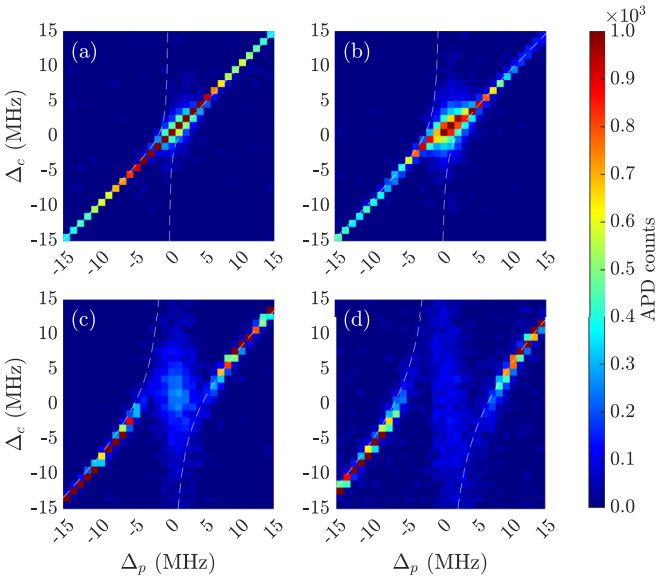

FIG. 3. Fluorescence from coupled atom-cavity states as a function of atom number. The effective atom numbers interacting with the cavity mode are (a) $N = 2000$, (b) $N = 5000$, (c) $N = 21\,250$, and (d) $N = 42\,500$, according to the fitted white dashed line. Fluorescence is counted for 10 s per pixel of the maps; the background from APD dark counts has been subtracted.

by the already observed central fluorescence maximum; for the smaller values of atom number, that feature masks the splitting to some extent.

The normal-mode splitting predicted by Eq. (13) is shown in Figs. 3(a)–3(d) as white dashed lines. The observations indicate that for the range of atom numbers that we are able to explore, we reach far into the collective strong-coupling regime, where the separation of the coupled resonances of the atom-cavity system is larger than the characteristic frequencies of all relevant broadening mechanisms.

C. Central feature in the fluorescence

In this section we investigate the fluorescence from the atoms with higher frequency resolution, in particular the central feature which, conspicuously, does not appear in the cavity transmission. In Fig. 4(a) the detected fluorescence is plotted as a function of probe-atom detuning when the cavity-atom detuning is set to zero. The laser frequency is scanned over the range $\Delta_\mathrm{p} = 2\pi \times (-6, \ldots, 6\ \mathrm{MHz})$ in steps of $2\pi \times 200$ kHz, and for each laser frequency the fluorescence photons are counted for 5 s. The measurement shows two peaks around ± 5 MHz and a broad peak centered around atomic resonance. The side peaks are understood as the atom-cavity coupled states, and their separation is described by $g_0\sqrt{N}$ [Eq. (13) with $\Delta_\mathrm{c} = 0$] corresponding to an effective atom number of 22 500. Our prediction from theory calculated using Eq. (12) is displayed in Fig. 4(b) and shows reasonable agreement with the experimental measurement.

We extend our understanding by spanning the cavity-atom detuning over the same range as the probe-atom detuning, with the same resolution. Figure 5(a) shows the measured fluorescence vs Δ_p and Δ_c. Figure 5(b) shows the corresponding

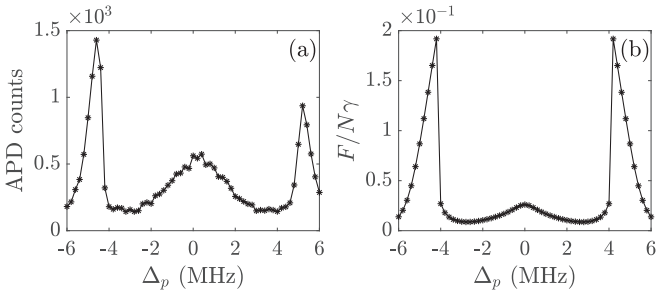

FIG. 4. Central fluorescence maximum. Atomic fluorescence is plotted as a function of laser detuning when the cavity is resonant to the atomic transition $\Delta_\mathrm{c} = 0$. (a) Measured photon counts using an APD vs probe laser frequency, with 200 kHz resolution. (b) Calculated fluorescence using Eq. (12), where an effective atom number of 22 500 is used with a cavity drive strength of $\eta = 2\pi \times 80$ MHz and inhomogeneous broadening of $\Delta\omega = 2\pi \times 0.62$ MHz.

excited-state population calculated from Eq. (12). Apart from the coupled states as in Fig. 2, the distinct peak around the atomic resonance is also visible. We find by exploring our theoretical model that its width increases with $\Delta\omega$; hence it is a consequence of the inhomogeneous broadening. It also requires significant driving strength, which indicates that it is a saturation feature. Remarkably, when introducing dephasing $\gamma_\mathrm{d} \sim \Delta\omega$ we find that this central maximum flattens out and becomes invisible. Detecting the feature in our experiment therefore indicates that inhomogeneous broadening exceeds the homogeneous dephasing rate in our experiment.

To understand the dependences of this central feature better we explore the fluorescence theoretically for various values of inhomogeneous broadening $\Delta\omega$, driving strength η, and dephasing rate γ_d. The results of this analysis are visible in Fig. 6. In all the cases, we look at the calculated fluorescence using Eq. (12) as a function of the probe frequency.

Figure 6(a) shows the influence of inhomogeneous broadening as we vary $\Delta\omega$ while γ_d and η are kept constant. As one observes, the width and visibility of the central feature increase for increasing $\Delta\omega$ while the normal-mode splitting is almost unaffected.

In Fig. 6(b) we study the effect of η for a given $\Delta\omega = 6\gamma$. Upon increasing η, one observes that the central feature

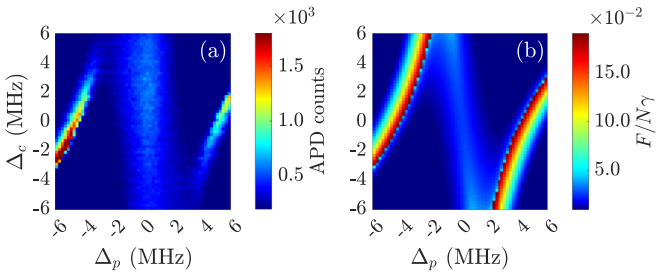

FIG. 5. Higher-resolution study of atomic fluorescence. (a) Measured and (b) calculated fluorescence are displayed vs Δ_c and Δ_p, exhibiting the atom-cavity coupled states alongside the broad resonance around $\Delta_\mathrm{p} = 0$. The parameters used for the calculation are the same as in Fig. 4. A frequency resolution of 200 kHz was used for both Δ_c and Δ_p.

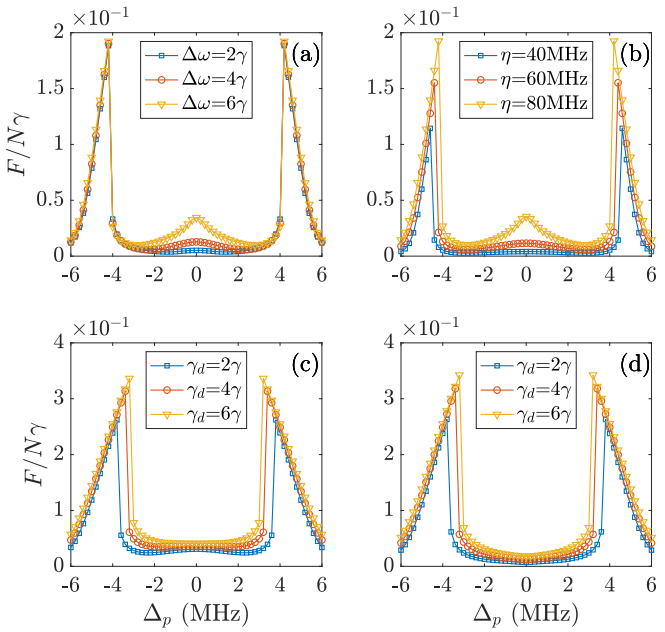

FIG. 6. Fluorescence calculated using Eq. (12) by varying different parameters as described below and for an effective atom number of 22 500 and as function of the detuning Δ_p. (a) Fluorescence for different $\Delta\omega$ (see the inset) for fixed $\gamma_d = 2\pi \times 1$ kHz and $\eta = 2\pi \times 80$ MHz. (b) Fluorescence for different values of η (see the inset) for $\Delta\omega = 6\gamma$ and $\gamma_d = 2\pi \times 1$ kHz. (c) Fluorescence for different values of γ_d (see the inset) for $\Delta\omega = 6\gamma$ and $\eta = 2\pi \times 80$ MHz. (d) Same plot and parameters as in (c) but for $\Delta\omega = \gamma$.

becomes more prominent, indicating the requirement for a strong drive to observe this feature, highlighting that one requires sufficient driving power.

Figure 6(c) shows the effect of homogeneous broadening in the form of dephasing on the fluorescence. To explore its effect we vary γ_d for fixed $\Delta\omega$ and η. The observation of the central feature relies on how big γ_d is relative to $\Delta\omega$. When γ_d is smaller than $\Delta\omega$ we observe the central feature. With increasing γ_d the central feature becomes less pronounced and for $\gamma_d = \Delta\omega$ it seems to disappear completely. We believe that this effect is an interplay of homogeneous and inhomogeneous broadening, as we explain now. For low dephasing rates each emitter has a very narrow emission frequency. In the fluorescence, however, we observe a broad central feature which comes from averaging many narrow emission profiles at different frequencies. The amount of fluorescence that is observed when driving at a given frequency is then in a first approximation determined by the number of emitters at that given frequency. In contrast, for dephasing rates that are comparable to the width $\Delta\omega$, one does not address individual narrow frequency classes since each emitter experiences a large homogeneous broadening. Consequently, one observes a washed-out signal that follows the rather flat signal visible in Fig. 6(c) for $\gamma_d = 6\gamma$.

To stress this competition between homogeneous and inhomogeneous broadening in our system even more, we show in Fig. 6(d) a calculation identical to that of in Fig. 6(c) but for small $\Delta\omega = \gamma$. Here the central feature is completely absent, highlighting the importance of inhomogeneous broadening to observe the central feature. We remark at this point that the possibility to observe this central feature in experiment is a consequence of working with narrow-linewidth atoms. We expect that in a similar experiment working with the blue transition, the broad line $\gamma_{\mathrm{MOT}} = 2\pi \times 29.1$ MHz would dominate inhomogeneous broadening, thus making the observation of the central feature impossible.

Before we conclude we would like to draw a connection between our results and the results in Ref. [65], where inhomogeneous broadening is understood as a form of disorder. By controlling and increasing the disorder strength, that work demonstrates how disorder can break strong collective coupling, making the previously dark states cross over to a distribution of so-called gray states that are visible by an enhanced cavity transmission close to resonance $\Delta_p \approx 0 \approx \Delta_c$. In our experiment disorder originates from the different frequencies of the individual atoms that result in inhomogeneous broadening. Note that even such a simple form of disorder already breaks the permutation symmetry in the Tavis-Cummings model, disallowing for a clear separation of bright and dark states. This form of disorder cannot be fully controlled in our experiment as it is a combination of several effects. Still, for large atom numbers for which we have the strongest collective coupling rate, we observe in the cavity transmission only the normal-mode splitting and almost no signal close to resonance. This hints towards the emergence of cavity-protected states, which have also been discussed in Ref. [64]. In the fluorescence, however, we observe a very clear signal in the form of a central feature. A possible explanation for this finding is the formation of correlated states with a significant number of atoms in the excited state that cannot emit into the cavity but can emit into free space. Our experiment could thus also be used to study disorder in collectively coupled models with two clear advancements. First, we are ultimately only limited by the very narrow transition line, which potentially allows us to resolve narrower features as in, for instance, Ref. [65]. Second, this is all achieved in a continuous (strong) driven-dissipative setting, which, on one hand, allows us to extract the information of the excited-state population because of the massively enhanced measurement time and, on the other hand, makes the physics even richer because one cannot rely on Hamiltonian descriptions.

V. CONCLUSION

In this work we have investigated the formation of atom-cavity dressed states in the collective strong-coupling regime on a narrow atomic line, while the atoms are trapped and cooled in a magneto-optical trap. The coupled states are observed in the cavity transmission as well as in free-space fluorescence, which enables us to simultaneously investigate their photonic character and their atomic character. A theoretical mean-field description reproduces the main features of the experimental observations. A broad atomic resonance which only appears in fluorescence is also found in the theory prediction, confirming our understanding. Hence it allows us to study how inhomogeneous broadening as a result of cooling and trapping on a much broader transition [66] can affect the atom-cavity interaction on the narrow line.

Our simplified theory models effects such as frequency broadening arising from atomic motion, due to magnetic-field gradients and fluctuations, and scattering of blue photons, by two simple mechanisms: inhomogeneous broadening introduced by $\Delta\omega$ and homogeneous dephasing described by γ_d. Despite these simplifications, we find satisfactory agreement between theory and experiment. In addition, it should be noted that the parameters used in the model calculations are consistent with other measurements on the same system [44,66].

Nevertheless, we do not find full quantitative agreement between the theory and the experiment. The most striking difference is visible in the dressed-state resonances, which are far more pronounced in the theory than they are in the experimental measurement. Our theory predicts stable dressed states even for driving frequencies close to resonance $\Delta_p \approx 0$. This is not found in the experiment and therefore requires refined modeling based on further measurements. One possibility might be a probe-frequency-dependent source of dephasing and broadening which is particularly pronounced close to atomic resonance. Such a mechanism might be related to optomechanical forces coming from the green laser light. While such forces may be expected to have even significant effects [1,3], they have not been considered in the present paper but are left for future work.

Our experiment and its modeling demonstrate an approach to study the formation and properties of atom-cavity states on a narrow line, far in the collective strong-coupling regime, and when the atoms are cooled and trapped continuously on a much (greater than 100 times) wider transition. Notably, we simultaneously investigate the photonic and the atomic character of the coupled states. Apart from the coupled states, we highlight a central resonance, visible only in the atomic signal, which allows us to draw conclusions regarding broadening and dephasing mechanisms in the atom-cavity system. Apart from fundamentally exploring collective latter-might phenomena, we expect our work to find significance, for example, in applications of narrow-line cavity coupling for ultrastable lasers or active atomic clocks.

ACKNOWLEDGMENTS

We gratefully acknowledge funding from the Deutsche Forschungsgemeinschaft (DFG) (German Research Foundation) through the Collaborative Research Center project QuCoLiMa, TRR-306, Subproject No. B04. We thank S. Schäffer, F. Fama, and T. Schmit for stimulating discussions. S.B.J. acknowledges support from the DFG through Collaborative Research Center project OSCAR, Grant No. TRR-185, Subprojects No. A4 and No. A5.

DATA AVAILABILITY

The data that support the findings of this article are openly available [67].

[1] P. Domokos and H. Ritsch, Phys. Rev. Lett. **89**, 253003 (2002).
[2] A. T. Black, H. W. Chan, and V. Vuletić, Phys. Rev. Lett. **91**, 203001 (2003).
[3] J. K. Asbóth, P. Domokos, H. Ritsch, and A. Vukics, Phys. Rev. A **72**, 053417 (2005).
[4] K. J. Arnold, M. P. Baden, and M. D. Barrett, Phys. Rev. Lett. **109**, 153002 (2012).
[5] H. Ritsch, P. Domokos, F. Brennecke, and T. Esslinger, Rev. Mod. Phys. **85**, 553 (2013).
[6] S. Schütz, S. B. Jäger, and G. Morigi, Phys. Rev. A **92**, 063808 (2015).
[7] M. Gross and S. Haroche, Phys. Rep. **93**, 301 (1982).
[8] K. Baumann, C. Guerlin, F. Brennecke, and T. Esslinger, Nature (London) **464**, 1301 (2010).
[9] W. Guerin, M. O. Araújo, and R. Kaiser, Phys. Rev. Lett. **116**, 083601 (2016).
[10] M. Gegg, A. Carmele, A. Knorr, and M. Richter, New J. Phys. **20**, 013006 (2018).
[11] M. A. Norcia, M. N. Winchester, J. R. K. Cline, and J. K. Thompson, Sci. Adv. **2**, e1601231 (2016).
[12] M. A. Norcia, J. R. K. Cline, J. A. Muniz, J. M. Robinson, R. B. Hutson, A. Goban, G. E. Marti, J. Ye, and J. K. Thompson, Phys. Rev. X **8**, 021036 (2018).
[13] J. Klinder, H. Keßler, M. Wolke, L. Mathey, and A. Hemmerich, Proc. Natl. Acad. Sci. USA **112**, 3290 (2015).
[14] T. Laske, H. Winter, and A. Hemmerich, Phys. Rev. Lett. **123**, 103601 (2019).
[15] A. Shankar, J. T. Reilly, S. B. Jäger, and M. J. Holland, Phys. Rev. Lett. **127**, 073603 (2021).
[16] M. A. Norcia, R. J. Lewis-Swan, J. R. K. Cline, B. Zhu, A. M. Rey, and J. K. Thompson, Science **361**, 259 (2018).
[17] B. P. Marsh, Y. Guo, R. M. Kroeze, S. Gopalakrishnan, S. Ganguli, J. Keeling, and B. L. Lev, Phys. Rev. X **11**, 021048 (2021).
[18] R. M. Kroeze, B. P. Marsh, D. A. Schuller, H. S. Hunt, S. Gopalakrishnan, J. Keeling, and B. L. Lev, arXiv:2311.04216.
[19] B. P. Marsh, R. M. Kroeze, S. Ganguli, S. Gopalakrishnan, J. Keeling, and B. L. Lev, Phys. Rev. X **14**, 011026 (2024).
[20] N. Defenu, T. Donner, T. Macrì, G. Pagano, S. Ruffo, and A. Trombettoni, Rev. Mod. Phys. **95**, 035002 (2023).
[21] V. Torggler, S. Krämer, and H. Ritsch, Phys. Rev. A **95**, 032310 (2017).
[22] E. Altman, K. R. Brown, G. Carleo, L. D. Carr, E. Demler, C. Chin, B. DeMarco, S. E. Economou, M. A. Eriksson, K.-M. C. Fu *et al.*, PRX Quantum **2**, 017003 (2021).
[23] M. Ye, Y. Tian, J. Lin, Y. Luo, J. You, J. Hu, W. Zhang, W. Chen, and X. Li, Phys. Rev. Lett. **131**, 103601 (2023).
[24] J. Chen, Chinese Sci. Bull. **54**, 348 (2009).
[25] D. Meiser, J. Ye, D. R. Carlson, and M. J. Holland, Phys. Rev. Lett. **102**, 163601 (2009).
[26] H. Liu, S. B. Jäger, X. Yu, S. Touzard, A. Shankar, M. J. Holland, and T. L. Nicholson, Phys. Rev. Lett. **125**, 253602 (2020).
[27] S. L. Kristensen, E. Bohr, J. Robinson-Tait, T. Zelevinsky, J. W. Thomsen, and J. H. Müller, Phys. Rev. Lett. **130**, 223402 (2023).
[28] E. A. Bohr, S. L. Kristensen, C. Hotter, S. A. Schäffer, J. Robinson-Tait, J. W. Thomsen, T. Zelevinsky, H.

Ritsch, and J. H. Müller, Nat. Commun. **15**, 1084 (2024).
[29] H. J. Metcalf and P. van der Straten, *Laser Cooling and Trapping*, Graduate Texts in Contemporary Physics (Springer, New York, 1999).
[30] C.-C. Chen, S. Bennetts, R. G. Escudero, B. Pasquiou, and F. Schreck, Phys. Rev. Appl. **12**, 044014 (2019).
[31] M. Tang, S. A. Schäffer, and J. H. Müller, Phys. Rev. A **106**, 063704 (2022).
[32] S. B. Jäger, H. Liu, J. Cooper, T. L. Nicholson, and M. J. Holland, Phys. Rev. A **104**, 033711 (2021).
[33] J. R. K. Cline, V. M. Schäfer, Z. Niu, D. J. Young, T. H. Yoon, and J. K. Thompson, Phys. Rev. Lett. **134**, 013403 (2025).
[34] C.-C. Chen, R. González Escudero, J. Minář, B. Pasquiou, S. Bennetts, and F. Schreck, Nature (London) **606**, 683 (2022).
[35] S. Dubey, G. A. Kazakov, B. Heizenreder, S. Zhou, S. Bennetts, S. A. Schäffer, A. Sitaram, and F. Schreck, Phys. Rev. Res. **7**, 013292 (2025).
[36] F. Famà, S. Zhou, B. Heizenreder, M. Tang, S. Bennetts, S. B. Jäger, S. A. Schäffer, and F. Schreck, Phys. Rev. A **110**, 063721 (2024).
[37] V. M. Schäfer, Z. Niu, J. R. K. Cline, D. J. Young, E. Y. Song, H. Ritsch, and J. K. Thompson, Nat. Phys. **21**, 902 (2025).
[38] T. Salzburger and H. Ritsch, Phys. Rev. Lett. **93**, 063002 (2004).
[39] T. Salzburger and H. Ritsch, Phys. Rev. A **74**, 033806 (2006).
[40] M. Xu, S. B. Jäger, S. Schütz, J. Cooper, G. Morigi, and M. J. Holland, Phys. Rev. Lett. **116**, 153002 (2016).
[41] S. B. Jäger, M. Xu, S. Schütz, M. J. Holland, and G. Morigi, Phys. Rev. A **95**, 063852 (2017).
[42] C. Hotter, D. Plankensteiner, L. Ostermann, and H. Ritsch, Opt. Express **27**, 31193 (2019).
[43] H. Gothe, D. Sholokhov, A. Breunig, M. Steinel, and J. Eschner, Phys. Rev. A **99**, 013415 (2019).
[44] H. Gothe, T. Valenzuela, M. Cristiani, and J. Eschner, Phys. Rev. A **99**, 013849 (2019).
[45] G. S. Agarwal, J. Opt. Soc. Am. B **2**, 480 (1985).
[46] Y. Zhu, D. J. Gauthier, S. E. Morin, Q. Wu, H. J. Carmichael, and T. W. Mossberg, Phys. Rev. Lett. **64**, 2499 (1990).
[47] R. J. Thompson, G. Rempe, and H. J. Kimble, Phys. Rev. Lett. **68**, 1132 (1992).
[48] M. Brune, F. Schmidt-Kaler, A. Maali, J. Dreyer, E. Hagley, J. M. Raimond, and S. Haroche, Phys. Rev. Lett. **76**, 1800 (1996).
[49] H. J. Kimble, Phys. Scr. **T76**, 127 (1998).
[50] J. McKeever, J. R. Buck, A. D. Boozer, and H. J. Kimble, Phys. Rev. Lett. **93**, 143601 (2004).
[51] I. Schuster, A. Kubanek, A. Fuhrmanek, T. Puppe, P. W. H. Pinkse, K. Murr, and G. Rempe, Nat. Phys. **4**, 382 (2008).
[52] M. Mücke, E. Figueroa, J. Bochmann, C. Hahn, K. Murr, S. Ritter, C. J. Villas-Boas, and G. Rempe, Nature (London) **465**, 755 (2010).
[53] J. Gripp, S. L. Mielke, and L. A. Orozco, Phys. Rev. A **56**, 3262 (1997).
[54] A. K. Tuchman, R. Long, G. Vrijsen, J. Boudet, J. Lee, and M. A. Kasevich, Phys. Rev. A **74**, 053821 (2006).
[55] E. Suarez, F. Carollo, I. Lesanovsky, B. Olmos, P. W. Courteille, and S. Slama, Phys. Rev. A **107**, 023714 (2023).
[56] M. G. Raizen, R. J. Thompson, R. J. Brecha, H. J. Kimble, and H. J. Carmichael, Phys. Rev. Lett. **63**, 240 (1989).
[57] B. T. R. Christensen, M. R. Henriksen, S. A. Schäffer, P. G. Westergaard, D. Tieri, J. Ye, M. J. Holland, and J. W. Thomsen, Phys. Rev. A **92**, 053820 (2015).
[58] D. Rivero, C. A. Pessoa, Jr., G. H. de França, R. C. Teixeira, S. Slama, and P. W. Courteille, New J. Phys. **25**, 093053 (2023).
[59] F. Rohde, M. Almendros, C. Schuck, J. Huwer, M. Hennrich, and J. Eschner, J. Phys. B **43**, 115401 (2010).
[60] H. Tanji-Suzuki, I. D. Leroux, M. H. Schleier-Smith, M. Cetina, A. T. Grier, J. Simon, and V. Vuletić, in *Advances in Atomic, Molecular, and Optical Physics*, edited by E. Arimondo, P. Berman, and C. Lin (Academic, New York, 2011), Vol. 60, pp. 201–237.
[61] T. Botzung, D. Hagenmüller, S. Schütz, J. Dubail, G. Pupillo, and J. Schachenmayer, Phys. Rev. B **102**, 144202 (2020).
[62] M. A. Zeb, Phys. Rev. A **106**, 063720 (2022).
[63] T. Gera and K. L. Sebastian, J. Chem. Phys. **156**, 194304 (2022).
[64] M. Baghdad, P.-A. Bourdel, S. Schwartz, F. Ferri, J. Reichel, and R. Long, Nat. Phys. **19**, 1104 (2023).
[65] N. Sauerwein, F. Orsi, P. Uhrich, S. Bandyopadhyay, F. Mattiotti, T. Cantat-Moltrecht, G. Pupillo, P. Hauke, and J.-P. Brantut, Nat. Phys. **19**, 1128 (2023).
[66] M. Cristiani, T. Valenzuela, H. Gothe, and J. Eschner, Phys. Rev. A **81**, 063416 (2010).
[67] J. Eschner, S. Shaju, and S. B. Jäger, Zenodo, Geneva, 2025, https://zenodo.org/records/1543543.